Receptor Imaging with Atrial Natriuretic Peptide Part 1: High Specific Activity Iodine-123-Atrial Natriuretic Peptide

Raymond Lambert, Roland Willenbrock, Johanne Tremblay, Gary Bavaria, Yves Langlois, Keith Hogan, Daniel Tartaglia, Richard J. Flanagan and Pavel Hamet

Centre de Recherche, Department of Nuclear Medicine, Department of Surgery, Department of Medicine, Hôtel-Dieu de Montréal, Université de Montréal; and Radiopharmaceutical Research and Development, Merck Frosst Canada Inc., Montréal, Québec, Canada

Methods: Atrial natriuretic peptide (ANP) was labeled in high specific activity using ^{123}I (p,2n). The biodistribution of ^{123}I-ANP was studied in green vervet monkeys by gamma scintigraphy and in rats by dissection and gamma counting. Iodine-125-ANP was also studied in monkeys by in vitro autoradiography. **Results:** Iodine-123-ANP showed rapid blood clearance with localization to ANP receptors in the kidneys and lungs, which accounted for 35% of total uptake. In vivo competition imaging studies using cold ANP$^{99-126}$ and C-ANP$^{102-121}$ proved that uptake is receptor mediated and allowed imaging of the differential biodistribution of A/B and C-ANP receptor families. Thus, it was possible through the use of selective receptor occupation to prevent uptake in certain organs and to effectively steer the labeled ANP to others. The observed biodistribution patterns were confirmed by an in vitro study using ^{125}I-ANP in the same monkeys, which correlated the scintigraphic images with receptor distribution. An in vivo biodistribution study in rats showed a profound effect of specific activity on biodistribution, with a cutoff for receptor uptake at less than 3000 Ci/mmole. **Conclusion:** Gamma scintigraphy with ^{123}I-ANP permits the imaging of ANP receptors in vivo. In contrast to receptor imaging with either organic molecules or antibodies, ANP provides rapid first-pass uptake and substantial accumulation (%dose/organ ≈ 20% or greater) in receptors. The key to receptor imaging with peptides is high specific activity. Labeled ANP offers potential as a diagnostic tool for diabetic nephropathy, particularly for quantifying the involvement of glomerular disease.

Key Words: atrial natriuretic peptide; receptor imaging

J Nucl Med 1994; 35:628–637

Atrial natriuretic peptide (ANP), a peptide hormone produced in the cardiac atrium, acts upon the kidney, playing an important role in fluid, electrolyte and blood pressure homeostasis (*1–5*). In vitro studies have demonstrated a high density of specific ANP receptors in the kidneys, adrenals and lungs (*6–8*). In the kidney, these receptors are most numerous in glomeruli (*7,9–13*).

Several types of ANP binding sites have been reported (*14–16*). Three different ANP receptors have now been cloned (*17–19*). A- and B-receptors contain particulate guanylate cyclase in their intracellular domain (*18,19*). The more abundant C-receptor is not coupled to guanylate cyclase (*20,21*), but it has 30% and 33% homology in the extracellular compartment with A- and B-receptors, respectively (*18,19*).

The biological responses to ANP have been correlated with elevated levels of cGMP (*22,23*) stimulated by guanylate cyclase (*12,24*), and A- and B-receptors containing this enzyme seem to express the peptide's biological actions. The function of the C-receptor is not yet fully known, but a clearing or buffering role has been postulated (*25,26*).

Existing methods in nuclear medicine for evaluating renal pathology consist of measuring either the glomerular filtration rate [diethylene-triaminepentaacetic acid (DTPA) and ethylenediaminetetraacetic acid (EDTA)], renal plasma flow (Hippuran), visualization of the kidney cortex by 2,3 dimercaptosuccinic acid (DMSA) or glucoheptonate (*27*). No substance for the specific visualization of glomeruli is presently available.

Currently, binding studies are always performed in vitro and there is no method for the in vivo analysis of ANP receptors in living creatures. ANP receptor up- and down-regulation has been reported in glomeruli (*13,28*), the adrenals, brain (*10*) and vascular smooth muscle cells (*29,30*). Abnormalities of ANP receptors in spontaneously hypertensive rats have been demonstrated in the kidneys (*31,32*) and adrenals (*33*). However, these studies have not distinguished the specific types of ANP receptors and their relevance for in vivo effects. We have recently briefly reported the first nuclear imaging of ANP receptors in vivo (*34*). We describe here a method which permits visualization of ANP receptors in live whole animals.

Received Aug. 5, 1993; revision accepted Dec. 29, 1993.

For correspondence or reprints contact: Dr. Pavel Hamet, Centre de Recherche Hôtel Dieu de Montréal, 3850 rue St-Urbain, Pavillon Marie de la Ferre, Montréal, Québec H2W 1T8, Canada.

MATERIALS AND METHODS

Materials

Synthetic rat ANP$^{99-126}$ was purchased from Institut Armand-Frappier (Laval, Quebec, Canada). Rat ANP$^{101-126}$ was synthesized by Dr. Ruth Nutt (Merck Sharp and Dohme Research Laboratories, Westpoint, PA). Rat C-ANP$^{102-121}$-des[Gln, Ser, Gly, Leu, Gly] (C-ANP) was generously donated by Thomas Maack (New York, NY). Carrier-free Na^{125}I was obtained from Amersham Corp. (Oakville, Ontario, Canada). Na^{123}I (^{123}Xe-p,2n ^{123}I) was donated by Frosst Radiopharmaceuticals (Pointe-Claire, Quebec). Lactoperoxidase was obtained from Sigma (St. Louis, MO) and the jackets, tethers and swivels from Alice Chatham, King Biomedical Arts (Los Angeles, CA).

Animals

Adult, male African green vervet monkeys, Cercopithecus aethiops (6–7 kg), were kept in individual stainless steel cages under a 12:12 hr light/dark cycle. They were given Purina primate chow supplemented with fresh food as well as tap water ad libitum. A silastic catheter (0.075 mm inner diameter, Dow Corning) was introduced into the external femoral vein and the catheter tip was advanced into the inferior vena cava. The catheter was externalized through the skin in the interscapular region, passed through a jacket and tether, and connected to an external swivel. It was maintained by daily flushing with heparinized saline and by a heparin lock. The animals were allowed to recover for at least 48 hr from the surgery before initiation of the experiment. The catheters were removed after 3 wk.

Male Sprague-Dawley rats (100–120 g) were purchased from Charles River Canada (St. Constant, Québec).

Labeling of ANP

Because of its shorter half-life (13 hr), in vivo studies were performed with ^{123}I-ANP which was prepared the same day. Iodine-125-ANP, which has a half-life of 60 days, was used for the in vitro studies. Rat ANP$^{99-126}$ was iodinated with ^{125}I by the slightly-modified lactoperoxidase method (*33*). Briefly, 20 μg of ANP, 5 mCi of ^{123}I, 5 μg of lactoperoxidase, 15 μl of hydrogen peroxide 30% and 50 μl of phosphate buffer were incubated at room temperature. After 5 min, 15 μl of hydrogen peroxide were added. This step was repeated twice with a 5-min incubation period after each hydrogen peroxide addition. Monoiodinated ANP was purified by HPLC on a C_{18} μ-Bondapak column by elution with a linear gradient of 20%–40% acetonitrile containing 0.1% trifluoroacetic acid at 0.5%/min and 1 ml/min. The specific activity of ^{125}I-ANP was 1500–2000 Ci/mmole.

ANP$^{101-126}$ was iodinated with ^{123}I using the chloramine-T method as follows: 10 μg of ANP$^{101-126}$ were dissolved in 40 μl of pH 7.8 borate buffer and 20 mCi of ^{123}I-sodium iodide added followed by 5 μg of chloramine-T in 5 μl of added water. The solution was vortexed at 0°C for 2 min and the reaction quenched with cysteine. The monoiodinated compound was isolated by HPLC as described above. The specific activity of ^{123}I-ANP was ≥50,000 Ci/mmole, this being the upper limit of measurement by HPLC/UV spectrometry at 218 nm.

Preparation of Organs and Solubilized Membranes

Kidneys, heart, lungs and liver were taken rapidly after decerebration from healthy, normotensive adult green vervet monkeys, weighed, cut into 1-cm slices, placed immediately in liquid nitrogen and kept at −70°C until required. The portion of these tissues that were reserved for membrane studies were homogenized three times with a Polytron for 20 sec, and the homogenized tissue was suspended in 50 m*M* Hepes buffer (pH 7.4) containing 1 m*M* ethylenediamine-tetraacetic acid (EDTA), 50 μg/ml leupeptin, 0.1 m*M* PMSF and 0.6 *M* KCl (buffer A) and centrifuged at 1500 g for 30 min. The supernatant was re-suspended in buffer A and centrifuged at 40,000 × g for 30 min. The pellet was again re-suspended in buffer A and centrifuged.

The tissue membranes were solubilized with Triton X-100 (3:1, U/V) for 60 min at 4°C in buffer A, then centrifuged at 100,000 × g for 2 min (*35*). The amount of solubilized proteins in the supernatant was measured by the method of Bradford.

Binding Studies

For competitive binding studies, 30 μg of solubilized membrane protein were incubated with increasing doses of unlabeled ANP (either rat ANP or C-ANP, 10^{-12} to 10^{-6} *M*) and ^{123}I-ANP (10×10^3 cpm). For saturation curves, increasing amounts of labeled ^{125}I-ANP ($1–100 \times 10^3$ cpm) were added to 30 μg of protein. For association/dissociation curves, the binding was stopped after different time periods ranging from 2 to 180 min. After 60 min, 10^{-6} *M* of unlabeled ANP was added and the dissociation measured at different time points. The reaction mixture (100 μl, pH 7.4) contained 200 m*M* of phosphate buffer, 20 μg/ml of aprotinin, 20 μg/ml of leupeptin, 10 m*M* of $MgCl_2$, 1 m*M* of PMSF, 0.8% of bovine serum albumin and 0.2% of Triton X-100. Nonspecific binding was measured by the addition of 1 μ*M* of unlabeled rat ANP$^{99-126}$. Binding was performed for 60 min (unless mentioned otherwise) at 22°C and stopped by adding 25 μl of gamma globulin 0.3% and by diluting the reaction sample with 1 ml of polyethyleneglycol (PEG, 16% in phosphate buffer, pH 7.4). The tube contents were immediately poured onto polyethylenimine-treated (0.3%, 30 min) glass fiber filters (Whatman GF/C), which were rinsed three times with 1 ml PEG. Radioactivity was counted with a gamma counter. The binding data were analyzed with the computer-based EBDA program (*36*), and the density and affinity of binding sites were determined with the LIGAND program (*37*).

Biodistribution Studies

A series of ^{123}I-ANP preparations at specific activities of 300 Ci/mmole, 3 kCi/mmole and 30 kCi/mmole were prepared by dilution of the radioactive material with unlabeled material. Approximately 1 μCi of each of these solutions was injected into male Sprague-Dawley rats in 0.5 ml of saline via the tail vein. The animals were killed at 1, 2, 5, 15 and 30 min postinjection and the major organs removed. These were rinsed in distilled water and counted in a Beckman 5500 gamma counter. The results were calculated as percent injected dose/organ as the average of five animals.

Nuclear Imaging

The animals were anesthetized with intramuscular ketamine (1 mg/kg) and xylazine (2 mg/kg), repeated about every 60 min as required, transported to the nuclear medicine department and positioned on a gamma camera in such a way as to provide a near full body scintigram. Iodine-123-ANP (500–700 μCi) and unlabeled ANP (when indicated) were diluted in 2 ml of saline and then injected intravenously as a bolus. The catheter was rinsed immediately with 10 ml of saline. A scintillation camera (Picker DDC300) and computer system (Picker PCS512) were used for data acquisition. Several regions of interest (ROIs) were followed (kidney, lung, liver, etc.). Data acquisition was started simultaneously with the injection of labeled ANP and continued for 180 min.

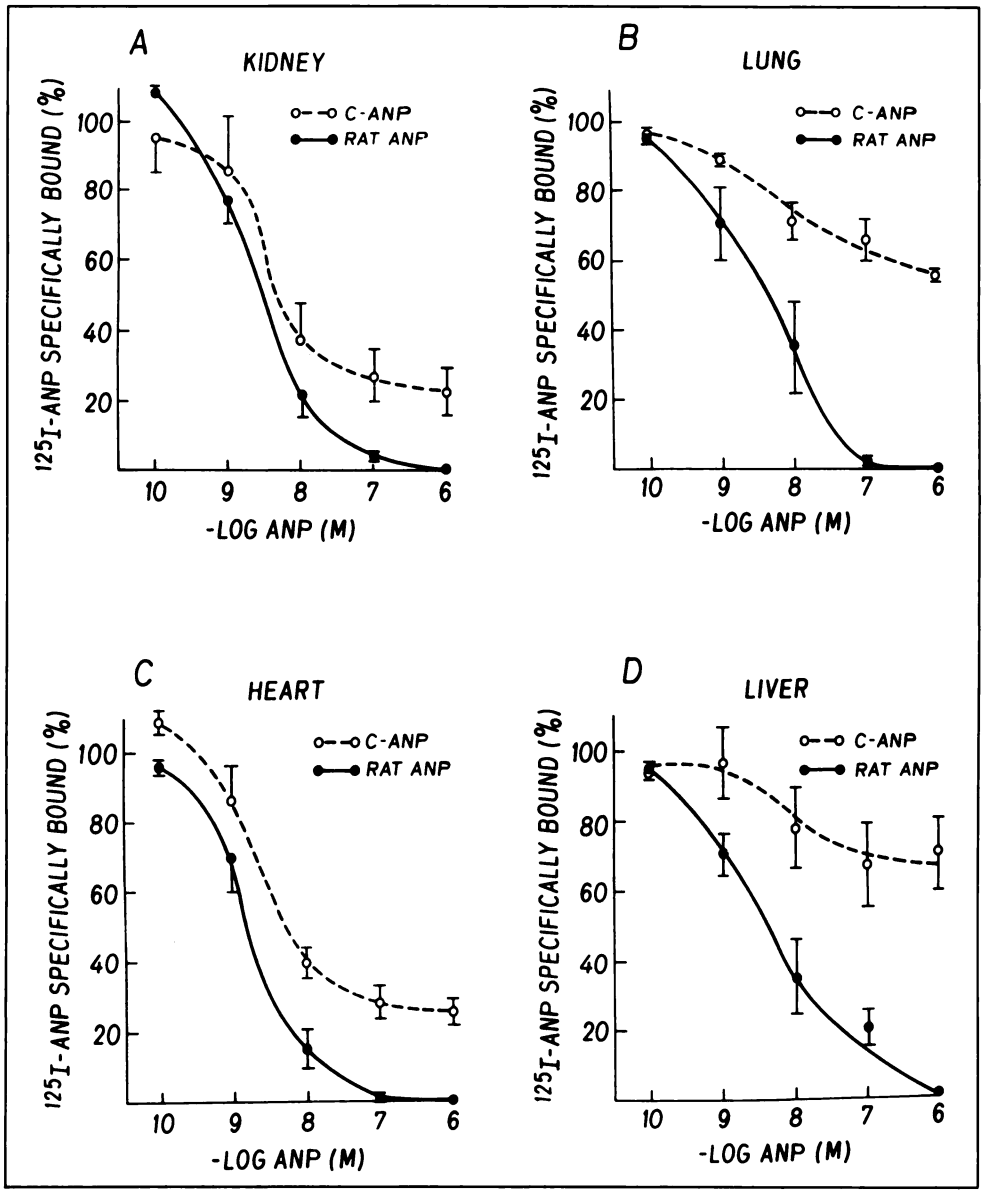

FIGURE 1. Displacement of ^{123}I-ANP with ANP$^{99-126}$ (continuous line) and C-ANP (interrupted line) on membranes prepared from monkeys in (A) kidney, (B) lung, (C) heart and (D) liver tissue. The ratio of C:A + B receptors can be determined from the ability of C-ANP to fully displace the bound radioactivity. Data are means ± s.e.m., n = 4.

RESULTS

In Vitro Binding of ANP to Membranes from Monkey Organs

Saturation Studies. The highest concentration of ANP receptors was found in kidney membranes with a B_{max} of 30.8 pmole/mg solubilized proteins. Lung and heart tissue had a B_{max} of 9.5 and 8.6 pmole/mg, respectively, while maximal binding capacity in the liver was only 4.2 pmole/mg. Dissociation curves showed that the binding of ANP to its receptors was virtually irreversible; dissociation of ANP from the receptor was 20% after 120 min as previously shown (*38*).

Competitive Binding with C-ANP. C-ANP binds exclusively to the C-receptor and cannot compete with ^{125}I-ANP at A- or B-receptors. Thus, the amount of labeled ANP which can be displaced by C-ANP corresponds to the proportion of C-receptors. In the kidney, the majority of ANP-binding sites were of the C-type as shown in Figure 1A where C-ANP (dotted line) displaced 77% of the total bound radioactivity while ANP displaced 100%. This also confirms our observations in rat glomeruli (*39*). C-receptors were also predominant in the heart (75%) (Fig. 1C). However, in the lung and liver, their proportion to guanylate cyclase-containing receptors was lower (44% and 30%, respectively) (Figs. 1B and D) and indicated by a lesser displacement with C-ANP.

Biodistribution Studies in Rats

There was a clear difference in the biodistribution of ^{123}I-ANP in rats at different specific activities as shown in Figure 2. At a specific activity of 300 Ci/mmole there was no uptake in the lung and only marginal uptake in the kidney. There was an obvious active uptake process at work at 3 kCi/mmole and 30 kCi/mmole in both lung and

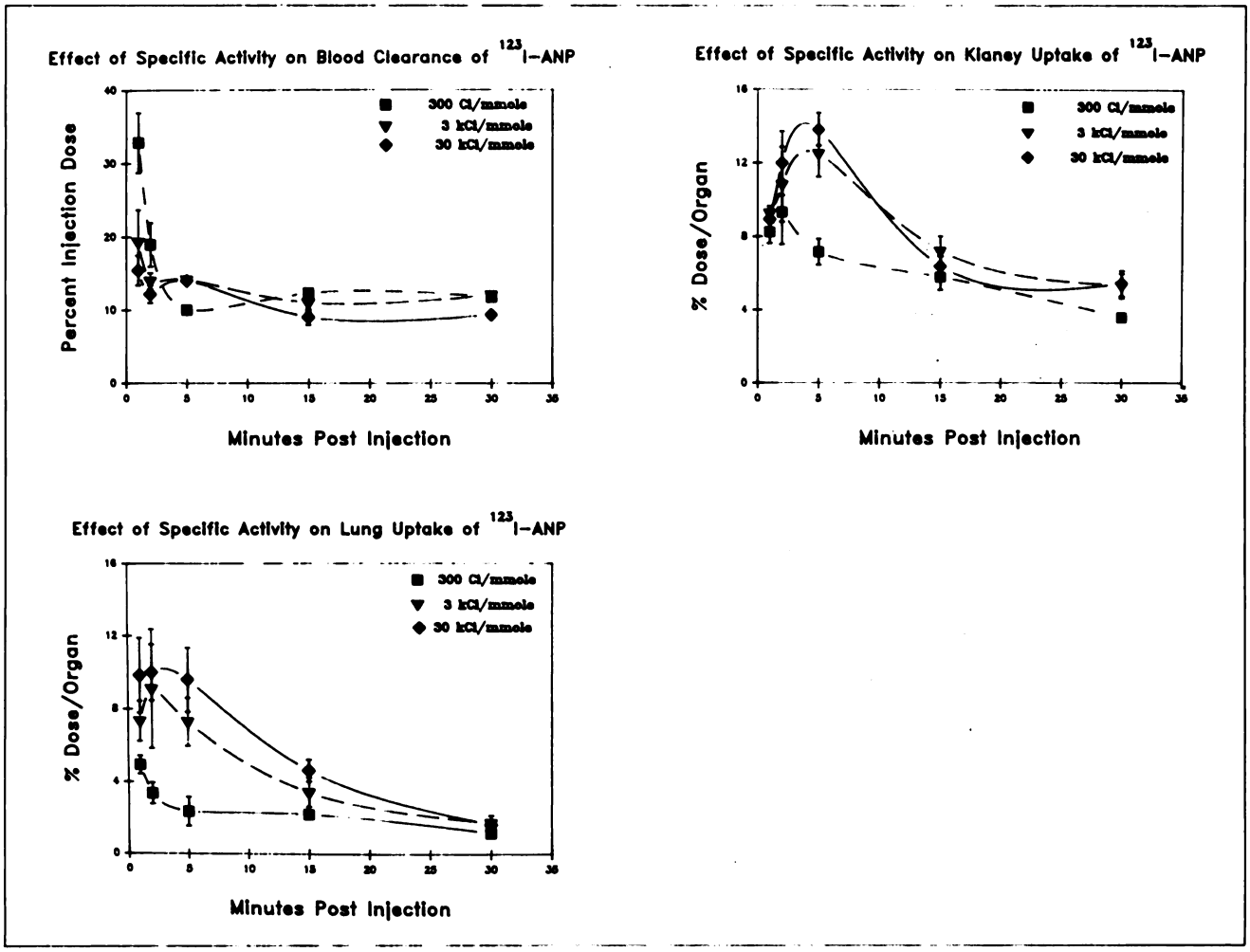

FIGURE 2. Percent dose/organ for ^{123}I-ANP in Sprague-Dawley rats after intravenous injection at various specific activities measured for lung, kidney and blood. The organs were removed after death at the specified times and counted in a gamma counter.

kidney. In the rat, lung uptake peaks at ≈3 min and in the kidney at ≈4.5 min. Clearance from the blood also shows a dependence on specific activity with the lower specific activity clearing more slowly.

Nuclear Imaging

Basal Uptake. Injection of ^{123}I-ANP into anesthetized monkeys resulted in rapid uptake in the kidneys and lungs. Figure 3A shows the images obtained after injection of ≈500 μCi ^{123}I-ANP (60–70 μCi/kg). Uptake in the kidneys was clearly evident in the first few minutes, while that in the lungs and liver was less pronounced. Radioactivity appeared in the bladder, salivary glands and thyroid after 30 min, but the kidneys were still the most densely labeled organs. Radioactivity decreased progressively in the kidneys and lungs during the second and third hours after injection, when the bladder became the most prominent region.

The %dose/organ for several organs is shown in Table 1. At 1 min, the kidney and lung represented over one-third of the total radioactivity measured (13.7% and 21.7%, respectively). Uptake by the liver was 5.8%, while radioactivity in the neck, bladder and arms showed low uniform distribution.

When normalized for the different size of ROIs, uptake per pixel (which is related to %dose/organ/g) was highest in the kidneys, followed by the lungs and liver (Fig. 4).

Competition Studies with ANP and C-ANP

Simultaneous injection of 20 μg of unlabeled ANP$^{99\text{-}126}$ with ^{123}I-ANP decreased uptake by the kidneys and increased lung and soft tissue labeling. Uptake by the bladder, thyroid and salivary glands appeared sooner. Little activity was measured in the kidneys after 1 hr, while the bladder, lungs and neck showed the greatest accumulation (*34*). These images are in sharp contrast to ^{123}I-ANP administration alone, when the kidney remained the dominant organ throughout the study period.

To investigate whether the individual receptor families could be differentiated, we simultaneously injected C-ANP, a specific C-receptor antagonist. As shown in Figure 3B, 100 μg of C-ANP resulted in an increased uptake in lung and soft tissue and decreased uptake in the kidneys. Soft tissue uptake was obvious after 10 min as was radio-

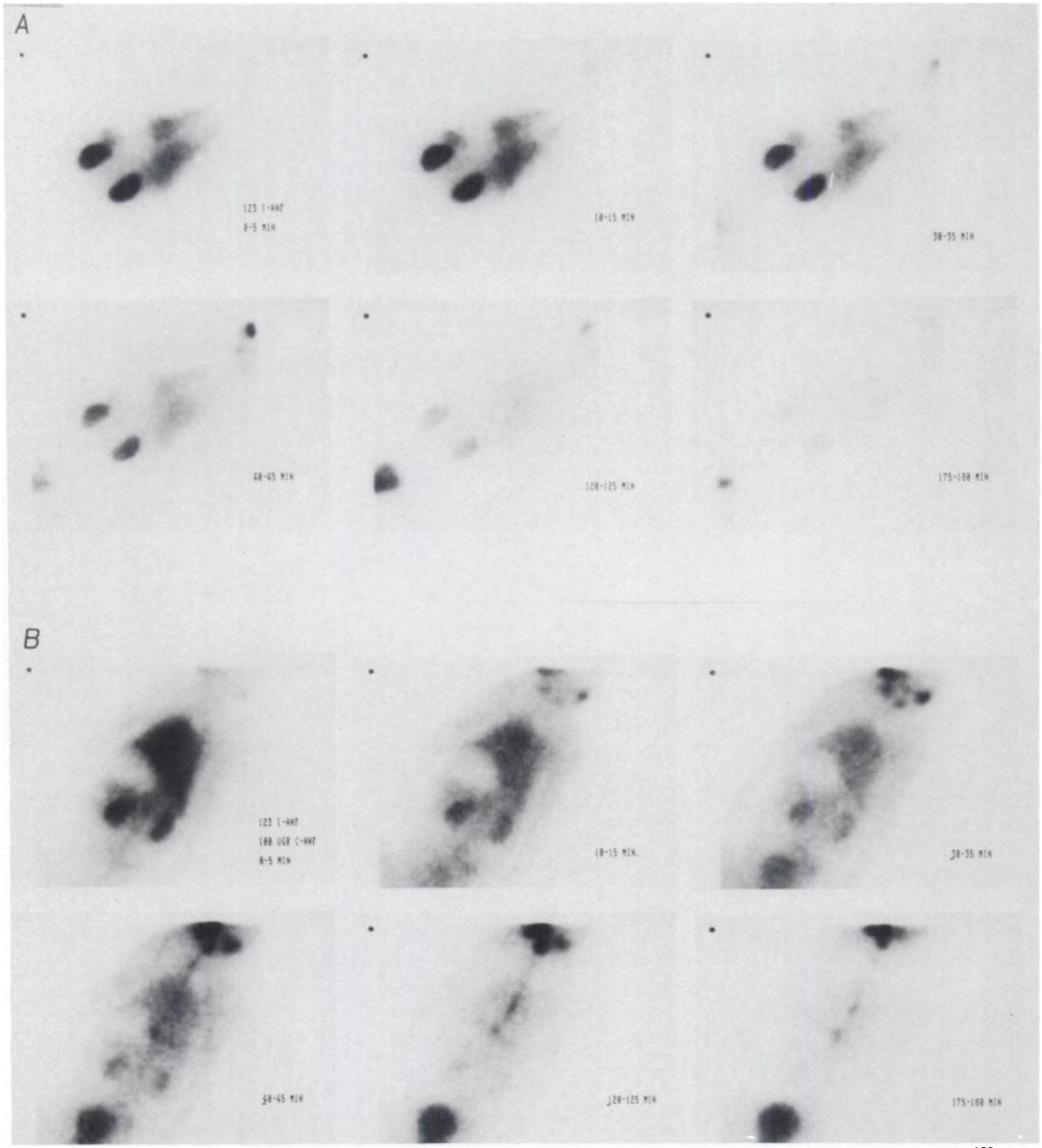

FIGURE 3. (A) Upper two rows show images obtained at 0–5, 10–15, 30–35, 60–65, 120–125, 175–180 min after injection of ^{123}I-ANP in monkeys in a basal state. Kidneys, lung and liver are clearly visualized. At later time periods, bladder and cervical uptake is observed. (B) The lower two rows show the effect of competition binding due to C-ANP at time periods after simultaneous injection of 100 μg unlabeled C-ANP and ^{123}I-ANP.

activity in the bladder. From 30 min onward, the thyroid, salivary glands and bladder were the most prominent regions.

When organ weights were taken into account, uptake per gram of tissue (Fig. 5) was higher in the lungs (weight: 33.0 g) and kidneys (32.8 g) than in the liver (174 g). With escalating C-ANP doses, uptake in the kidney declined, but increased in the lungs and remained unchanged in the liver.

ANP metabolism is still not fully understood, but it

TABLE 1
Uptake in Different Organs After Single ^{123}I-ANP Injection

Time (min)	Region								
	Kidney		Lung					Arm	
	Left	Right	Left	Right	Liver	Neck	Bladder	Left	Right
1	6.6 ± 0.4	7.1 ± 0.1	10.1 ± 0.6	11.6 ± 0.5	5.8 ± 0.5	2.6 ± 0.6	2.6 ± 0.2	3.0 ± 0.1	3.1 ± 0.1
15	6.3 ± 0.4	6.5 ± 0.1	8.8 ± 0.5	10.5 ± 1.2	5.7 ± 0.5	2.6 ± 0.6	3.1 ± 0.5	3.0 ± 0.1	3.4 ± 0.1

Data are means ± s.e.m. of percent injected dose in four separate experiments with three different monkeys.

involves degradation by proteolytic enzymes (*40–42*). Labeled ANP can be degraded into peptide fragments, tyrosine-bound iodine (*42*) and free iodine. One minute after ^{123}I-ANP injection, activity (per pixel) in the bladder at 0.016% was indistinguishable from soft tissue uptake, rising to 0.026% and 0.031% after 40–60 min, respectively. The simultaneous injection of unlabeled ANP$^{99-126}$ or of C-ANP doubled uptake after 1 min (Fig. 3B).

Analysis of Half-life

Figure 6 shows the activity curves obtained from four different regions after single ^{123}I-ANP doses and after simultaneous injection of 20 μg of ANP$^{99-126}$ in the same monkey obtained from a separate experiment. With ^{123}I-ANP, excretion was monoexponential in the kidney, lungs and liver but with simultaneous injection of unlabeled ANP$^{99-126}$, an additional first phase with a rapid decline was apparent. In contrast, the decay curve in soft tissue was linear and not much altered by unlabeled ANP in keeping with the nonspecific nature of this uptake. The half-life of ^{123}I-ANP in the kidneys, lungs and liver are shown in Table 2. When either ANP$^{99-126}$ or C-ANP were injected simultaneously, a second compartment was observed in all organs. The size of this component increased with increasing doses of C-ANP. The highest amount of C-ANP (100 μg) led to the appearance of a third compartment with a half-life of less than 60 sec.

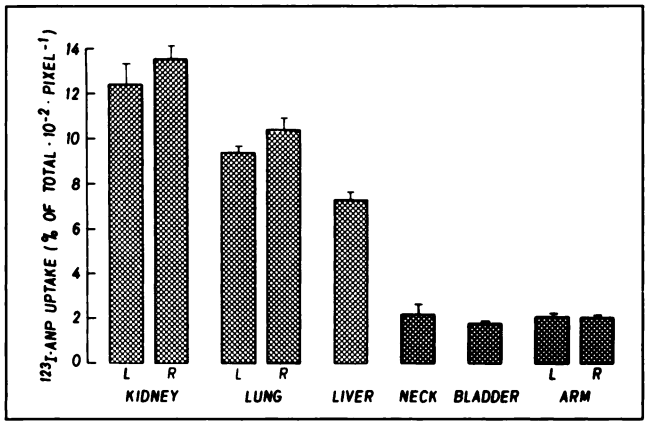

FIGURE 4. Relative uptake of ^{123}I-ANP in monkeys normalized per pixel (31 mm^2) in kidney, lung, liver, neck, bladder and arm. L = left, R = right. Data are the means ± s.e.m. of four separate experiments in three different animals.

DISCUSSION

Receptor imaging has been the focus of much research in recent years. Many of the early efforts at receptor imaging were based on the use of labeled steroids or synthetic organic molecules which behaved as agonists or antagonists. The use of ^{125}I-labeled peptides for in vitro receptor studies is a well recognized art which has not been transferred to in vivo receptor studies due to the rapid destruction of peptides in vivo by proteases. The half-life of circulating ANP is reported to be 20–40 sec in the rat (*12*), 1 min in the dog (*13*) and 3–5 min in humans (*14*). It is expected to be less than 1 min in these monkeys (6–7 kg). Since the heart can deliver ANP to the kidneys despite the presence of these proteases, it seems reasonable to assume that the same can be achieved with radiolabeled ligands.

Two modes of ANP metabolism have been described: binding to receptors followed by internalization (*40,41*), and degradation by endopeptidases (*42,43*). The major degrading enzyme, endopeptidase-24.11 (EC 3.4.24.11) (*45*),

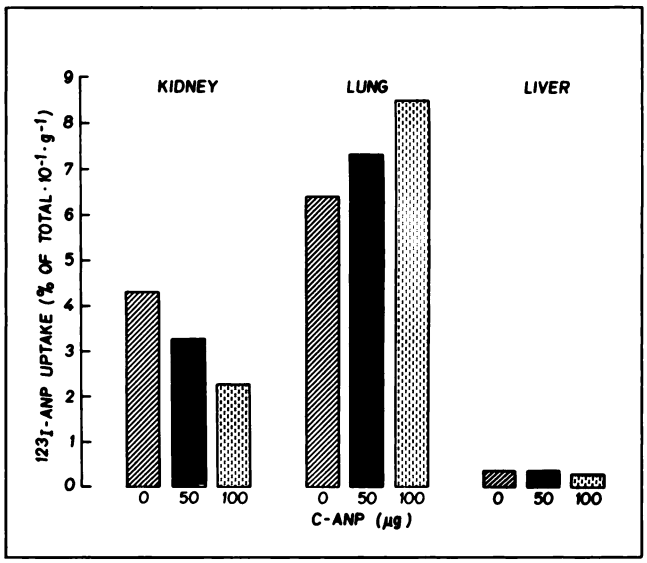

FIGURE 5. Organ uptake of ^{123}I-ANP in an individual green vervet monkey expressed as per gram tissue in kidney, lung and liver without and with simultaneous injection of 50 and 100 μg C-ANP. Uptake was measured in vitro after injection of ^{123}I-ANP, followed by euthanization after 5 min and organ removal. Radioactivity was measured by gamma counting of homogenized tissues. Data are based on two lungs and kidneys.

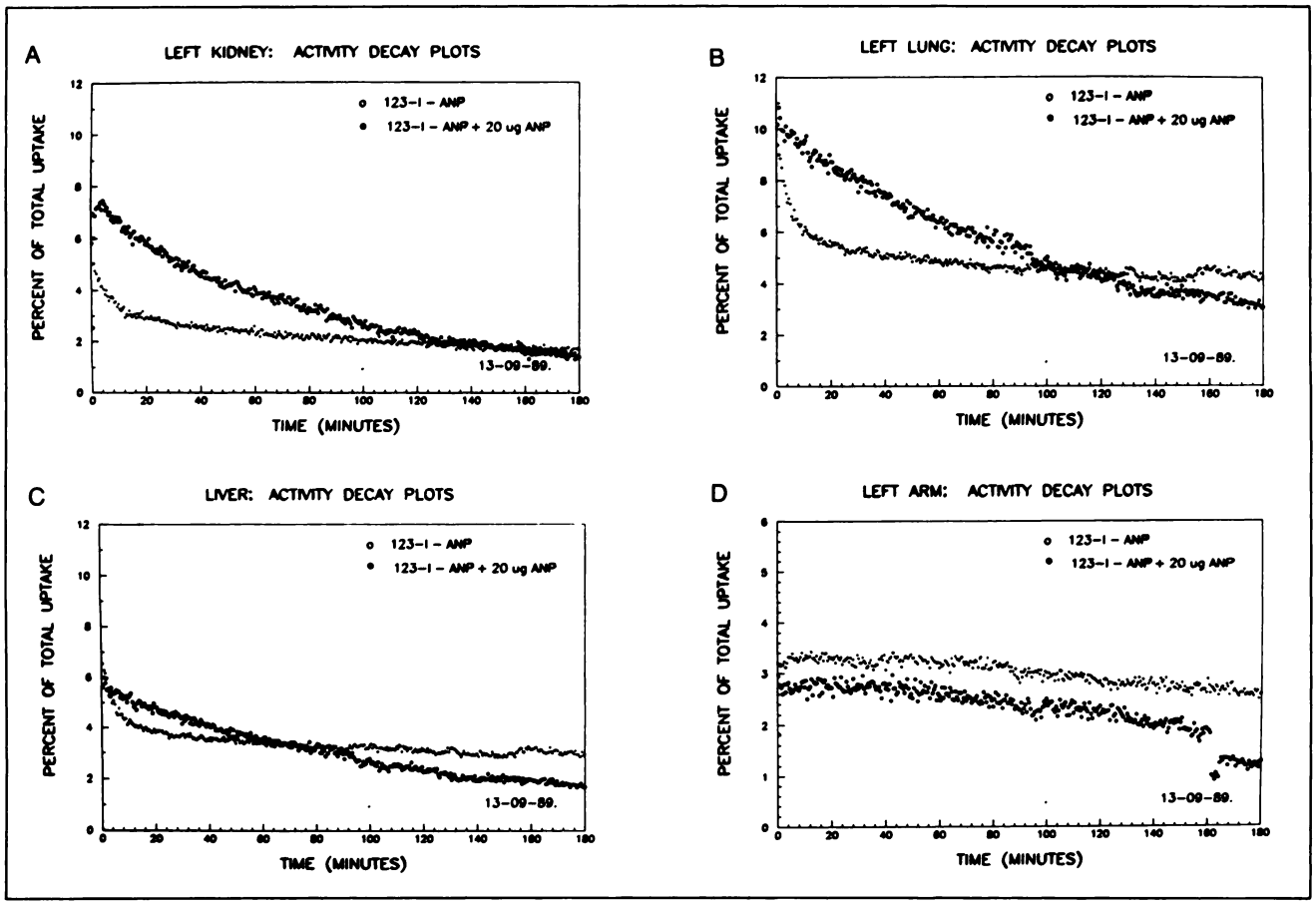

FIGURE 6. Activity decay curves of ^{123}I-ANP in (A) left kidney, (B) left lung, (C) liver and (D) left arm after injection of ^{123}I-ANP in monkey alone and simultaneously with 20 μg ANP$^{99-126}$. The least square fit curves shown were later used for half-life analysis.

is located at its highest concentrations in the renal brush border (*43,46*) but also exists in the lymph nodes, jejunum, adrenals and lungs (*47*). This enzyme has a K_m of 6.7 μM at pH 7.4 (*42*), more than 1000 times higher than the K_d for ANP receptors, which is between 50 and 500 p*M* (*6,13*). The enzyme probably plays a role in ANP degradation as specific inhibitors enhance the effect of ANP infusions (*42,48–50*) and increase cGMP levels in urine (*51*) and plasma (*52*).

Three ANP receptor types, A-, B- and C-receptors, have been identified and cloned. A- and B-receptors contain particulate guanylate cyclase (*18,19*) with cGMP mediating

TABLE 2
Analysis of Half-life and Identification of Compartments

Unlabeled compound	Dose (μg)	Kidney		Lung		Liver	
		%ID	min	%ID	min	%ID	min
None	0	100 ± 4	56 ± 1	100 ± 4	95 ± 2	100 ± 6	43 ± 4
ANP	20	46 ± 2	68 ± 5	41 ± 3	70 ± 7	40 ± 2	43 ± 4
		54 ± 5	3 ± 0.3	59 ± 7	3.0 ± 0.3	60 ± 5	2.0 ± 0.5
C-ANP	20	67 ± 2	53 ± 5	38 ± 1	64 ± 6	62 ± 2	46 ± 5
		33 ± 3	3 ± 0.3	35 ± 2	4.0 ± 0.5	38 ± 3	3.0 ± 0.4
				27 ± 4	0.4 ± 0.2		
	50	81 ± 3	61 ± 1	23 ± 1	49 ± 5	76 ± 2	37 ± 3
		19 ± 3	5.0 ± 0.5	14 ± 2	5.0 ± 0.6	24 ± 4	3.0 ± 0.4
				63 ± 5	0.3 ± 0.1		
	100	50 ± 2	107 ± 14	31 ± 1	117 ± 8	53 ± 9	57 ± 3
		27 ± 3	5.0 ± 0.6	33 ± 2	5.0 ± 0.4	47 ± 6	3.0 ± 0.2
		23 ± 5	0.4 ± 0.2	36 ± 4	0.5 ± 0.1		

The half-lives of ANP in different regions of interest are indicated in min ± s.d. from the fitting curve. The amplitudes are expressed in % ± s.d.

ANP's biological actions (*23*), while C-receptors (*17*) are believed to have a clearance function (*25*). ANP infusions elevate cGMP levels in plasma and urine (*22*), even at doses that do not yet elicit a biological effect (*44*).

The doses of ^{123}I-ANP injected here (0.3 ng/kg) were less than those required to increase cGMP or to elicit a biological action (*44*). Thus, they were likely to occupy a very small proportion of the receptors. Since binding to the receptor is more favorable than to the enzyme (by a factor of 1000), we can effectively avoid degradation of the radiolabel due to proteases. Thus, we can predict that specific activity will play a major role in the pattern of biodistribution, with receptor uptake decreasing with declining specific activity.

Our in vitro studies with monkey tissues showed that the greatest density of ANP receptors (at least in the monkey) is in the kidney, followed by the lungs and liver. Assuming that solubilized proteins constitute ≈40% of cell weight, the amount of ANP required to saturate the corresponding receptors can be calculated as being ≈0.4 μM for the kidney (i.e., 32.8 g × 30.8 pmole/mg × 0.4), ≈0.13 μM for the lung and ≈0.6 μM for the liver. For a 2-mCi dose of ANP, this corresponds to a specific activity of ≈2 Ci/mmole. While it is difficult to predict the effect that circulation or receptor occupancy might have on this value, we might anticipate that for optimal receptor imaging values 10^2–10^3 times higher would be needed. Assuming the dose will occupy <5% of the available receptor sites, this corresponds to at least 400 Ci/mmole.

The in vivo biodistribution results found in the rat (Fig. 2) confirm the role that specific activity plays in avoiding proteolytic destruction. At 3 kCi/mmole and above, the biodistribution is receptor mediated and at 300 Ci/mmole and below, it is nonspecific in nature.

Gamma scintigraphy rapidly and selectively visualized the kidneys and lungs of the green vervet monkey. The relative uptake of labeled ANP per surface area (pixel) was highest in the kidneys, in conformity with in vitro binding studies showing the highest ANP receptor density in this organ (30.8 pmole/mg protein) as compared to the lungs (9.5 pmole/mg protein) (Fig. 3A). We have previously shown that occupation of ANP receptors after simultaneous injection of unlabeled ANP$^{99\text{-}126}$ diminished binding of the labeled compound to the kidneys and lungs (*34*). It was also possible to image the distribution of ANP C-receptors by competitive binding studies with C-ANP, a selective C-receptor analog. This showed that the proportion of this receptor relative to the guanylate cyclase-containing receptors (A and B) varied from tissue to tissue, confirming previous results (*25*). In monkeys, the kidneys, which had the highest receptor density of all organs analyzed, possessed about 80% of C-receptors, while the lungs (30%) and liver (50%) had a smaller proportion of this receptor type. Selective inhibition of C-receptors with unlabeled C-ANP diminished the uptake of ^{123}I-ANP in the kidneys and not in the lung. This is due to the different ratios of C- and A/B-receptors in the kidneys and lungs. This confirms the specificity of nuclear imaging to selectively visualize different receptor types and shows that the presence of specific receptors in these organs is a reflection of in vivo binding, as suggested previously (*34*).

The half-life of tissue-bound ANP was easily estimated from the dynamic nuclear images obtained with ^{123}I-ANP. In the major target organs investigated, the half-life was between 40 and 90 min. This compartment probably represents binding, internalization and degradation by the ANP receptor, and we therefore tentatively called it the receptor compartment. When unlabeled ANP$^{99\text{-}126}$ or C-ANP is administered at the same time, another compartment with a short half-life of 3–5 min appears. We suggest that this represents an enzymatic compartment, probably including membrane-bound endopeptidases, such as EC 3.4.24.11. Because of its much higher K_m of over 10^{-6} M, it becomes relevant only when specific ANP receptors are occupied. Turnover at this enzymatic site will be much faster, with the second compartment having a half-life of only a few minutes. The earlier appearance of radioactivity in the bladder, thyroid and salivary glands with simultaneous injection of unlabeled ANP$^{99\text{-}126}$ or C-ANP supports this hypothesis (Fig. 3B).

Upon simultaneous injection of 100 μg of C-ANP, a third compartment with a half-life of less than 1 min appeared in the kidney, while in the lungs it was present even at lower doses of C-ANP. In all likelihood, it is a vascular flow compartment. At this high dose of ANP, it is expected that the unlabeled compound exerts its biological activity, which may contribute to the appearance of the third compartment.

CONCLUSION

We have described here a simple method for the in vivo real-time analysis of ANP receptors. We believe that our success derives in part from the nature of the receptor family (i.e., high affinity and large circulatory access) but also from the very high specific activity obtained from the use of p,2n I^{123}, NaI. This material is of much higher specific activity from that obtainable with I^{125} (2 kCi/mmole), I^{131} (2.5 kCi/mmole) and p,5n I^{123} (5 kCi/mmole). This high specific activity allowed the injection of extremely small amounts of ANP, such that binding to the small quantity of high-affinity ANP receptors could take place in the absence of binding to the rather large amount of low-affinity endopeptidase enzyme. Thus, localization in the receptor was rapid and mimicked the normal pattern of ANP uptake and metabolism. It seems likely that the same technique should be applicable to other peripheral receptor/peptide families.

Our approach makes possible the in vivo study of ANP receptors in different physiological or pathological states. This is a method with potential to visualize glomeruli in vivo and should be a candidate for clinical and diagnostic applications in diseases such as diabetic nephropathy and renovascular stenosis. The potential of this approach to

distinguish the progressive stages of glomerular involvement will deserve particular attention (*53*). In the lung, further research is needed to determine the cell types possessing ANP receptors but chronic obstructive and fibrotic diseases will be potential targets for this new imaging technique.

ACKNOWLEDGMENTS

This work was supported by a University-Industry grant (UI-12006) from Medical Research Council of Canada and Merck Frosst Canada, Inc.

The authors thank Régis Tremblay for his excellent technical assistance; Daniel Larin, Mario Vendette and Suzanne Cariotto for their valuable help; Dr. Roberta Palmour for her advice on monkeys; and Louise Chevrefils for her secretarial skills.

REFERENCES

1. Inagami T. Atrial natriuretic factor. *J Biol Chem* 1989;264:3043–3046.
2. Atlas SA, Laragh JH. Atrial natriuretic peptide: a new factor in hormonal control of blood pressure and electrolyte homeostasis. *Ann Rev Med* 1986; 37:397–414.
3. Genest J, Cantin M. Atrial natriuretic factor. *Circulation* 1987;75(suppl I):1118–1124.
4. Needleman P, Greenwald JE. Atriopeptin: a cardiac hormone intimately involved in fluid, electrolyte, and blood-pressure homeostasis. *N Engl J Med* 1986;314:828–834.
5. De Bold AJ. Atrial natriuretic factor: a hormone produced by the heart. *Science* 1985;230:767–770.
6. Napier MA, Vandlen RL, Albers-Schonberg G, et al. Specific membrane receptors for atrial natriuretic factor in renal and vascular tissues. *Proc Natl Acad Sci USA* 1984;81:5946–5950.
7. De Lean A, Vinay P, Cantin M. Distribution of atrial natriuretic factor receptors in dog kidney fractions. *FEBS Lett* 1985;193:239–242.
8. Olins GM, Patton DR, Tjoeng FS, Blehm DJ. Specific receptors for atriopeptin III in rabbit lung. *Biochem Biophys Res Commun* 1986;140:302–307.
9. Koseki C, Hayashi Y, Torikai S, Furuya M, Ohnuma N, Imai M. Localization of binding sites for alpha-rat atrial natriuretic polypeptide in rat kidney. *Am J Physiol* 1986;250:F210–F216.
10. Lynch DR, Brass KM, Snyder SH. Atrial natriuretic factor receptors in rat kidney, adrenal gland, and brain: autoradiographic localization and fluid balance dependent changes. *Proc Natl Acad Sci USA* 1986;83:3357–3361.
11. Healy DP, Fanestil DD. Localization of atrial natriuretic peptide binding sites within the rat kidney. *Am J Physiol* 1986;250:F573–F578.
12. Tremblay J, Gerzer R, Vinay P, Pang SC, Beliveau R, Hamet P. The increase of cGMP by atrial natriuretic factor correlates with the distribution of particulate guanylate cyclase. *FEBS Lett* 1985;181:17–22.
13. Ballermann BJ, Hoover RL, Karnovsky MJ, Brenner BM. Physiologic regulation of atrial natriuretic peptide receptors in rat renal glomeruli. *J Clin Invest* 1985;76:2049–2056.
14. Leitman DC, Andresen JW, Kuno T, Kamisaki Y, Chang JK, Murad F. Identification of multiple binding sites for atrial natriuretic factor by affinity cross-linking in cultured endothelial cells. *J Biol Chem* 1986;261:11650–11655.
15. Scarborough RM, Schenk DB, McEnroe GA, et al. Truncated atrial natriuretic peptide analogs. *J Biol Chem* 1986;261:12960–12964.
16. Takayanagi R, Inagami T, Snajdar RM, Imada T, Tamura M, Misono KS. Two distinct forms of receptors for atrial natriuretic factor in bovine adrenocortical cells. *J Biol Chem* 1987;262:12104–12113.
17. Fuller F, Porter JG, Arfsten BE, et al. Atrial natriuretic peptide clearance receptor. *J Biol Chem* 1988;269:9395–9401.
18. Chinkers M, Garbers DL, Chang MS, et al. A membrane form of guanylate cyclase is an atrial natriuretic peptide receptor. *Nature* 1989;338:78–83.
19. Chang M-S, Lowe DG, Lewis M, Hellmiss R, Chen E, Goedel DV. Differential activation by atrial and brain natriuretic peptides of two different receptor guanylate cyclases. *Nature* 1989;341:68–72.
20. Takayanagi R, Snajdar RM, Imada T, et al. Purification and characterization of two types of atrial natriuretic factor receptors from bovine adrenal cortex: guanylate cyclase-linked and cyclase-free receptors. *Biochem Biophys Res Commun* 1987;144:244–250.
21. Leitman DC, Andresen JW, Catalano RM, Waldman SA, Tuan JJ, Murad F. Atrial natriuretic peptide binding, cross-linking, and stimulation of cyclic GMP accumulation and particulate guanylate cyclase activity in cultured cells. *J Biol Chem* 1988;263:3720–3728.
22. Hamet P, Tremblay J, Pang SC, et al. Cyclic GMP as mediator and biological marker of atrial natriuretic factor. *J Hypertens* 1986;4(suppl 2):S49–S56.
23. Hamet P, Tremblay J, Pang SC, et al. Effect of native and synthetic atrial natriuretic factor on cyclic GMP. *Biochem Biophys Res Commun* 1984;123: 515–527.
24. Waldman SA, Rapoport RM, Murad F. Atrial natriuretic factor selectively activates particulate guanylate cyclase and elevates cyclic GMP in rat tissues. *J Biol Chem* 1984;259:14332–14334.
25. Maack T, Suzuki M, Almeida FA, et al. Physiological role of silent receptors of atrial natriuretic factor. *Science* 1987;238:675–678.
26. Almeida FA, Suzuki M, Scarborough RM, Lewicki JA, Maack T. Clearance function of type C receptors of atrial natriuretic factor in rats. *Am J Physiol* 1989;256:R469–R475.
27. Chervu LR, Blaufox MD. Renal radiopharmaceuticals—an update. *Semin Nucl Med* 1982;12:224–245.
28. Gauquelin G, Garcia R, Carrier F, et al. Glomerular ANF receptor regulation during changes in sodium and water metabolism. *Am J Physiol* 1988; 254:F51–F55.
29. Hirata Y, Tomita M, Takada S, Yoshimi H. Vascular receptor binding activities and cyclic GMP responses by synthetic human and rat atrial natriuretic peptides (ANP) and receptor down-regulation by ANP. *Biochem Biophys Res Commun* 1985;128:538–546.
30. Hughes RJ, Struthers RS, Fong AM, Insel PA. Regulation of the atrial natriuretic peptide receptor on a smooth muscle cell. *Am J Physiol* 1987; 253:C809–C816.
31. Swithers SE, Stewart RE, McCarty R. Binding sites for atrial natriuretic factor (ANF) in kidneys and adrenal glands of spontaneously hypertensive (SHR) rats. *Life Sci* 1987;40:1673–1681.
32. Garcia R, Gauquelin G, Thibault G, Cantin M, Schiffrin EL. Glomerular atrial natriuretic factor receptors in spontaneously hypertensive rats. *Hypertension* 1989;13:567–574.
33. Gutkowska J, Genest J, Thibault G, et al. Circulating forms and radioimmunoassay of atrial natriuretic factor. In: Rosenblatt M, Jacobs JW, eds. *Endocrinology and metabolism clinics of North America, Vol. 16, atrial natriuretic factor.* Philadelphia: W.B. Saunders Company; 1987:183–198.
34. Willenbrock R, Lambert R, Tremblay J, et al. In vivo measurement of atrial natriuretic peptide receptors using nuclear imaging. *Am J Hypertens* 1992; 5:832–836.
35. Tremblay J, Gerzer R, Pang SC, Cantin M, Genest J, Hamet P. ANF stimulation of detergent-dispersed particulate guanylate cyclase from bovine adrenal cortex. *FEBS Lett* 1986;194:210–214.
36. McPherson GA. Analysis of radioligand binding experiments—a collection of computer programs for the IBM PC. *J Pharmacol Methods* 1985;14:213–228.
37. Munson PJ, Rodbard D. Ligand: a versatile computerized approach for characterization of ligand-binding systems. *Anal Biochem* 1980;107:220–239.
38. Tremblay J, Willenbrock R, Cusson JR, et al. Role of particulate guanylate cyclase activation in the expression of the biological action of ANF. In: *Biological and molecular aspects of atrial factors.* New York: Alan R. Liss, Inc.; 1988:97–108.
39. Willenbrock RC, Tremblay J, Hamet P. Increased response of glomerular guanylate cyclase to ANF in spontaneously hypertensive rats. *FASEB J* 1989;3:A551.
40. Hirata Y, Takata S, Tomita M, Takaichi S. Binding, internalization, and degradation of atrial natriuretic peptide in cultured vascular smooth muscle cells of rat. *Biochem Biophys Res Commun* 1985;132:976–984.
41. Hughes RJ, Struthers RS, Fong AL, Insel PA. Receptor-induced degradation of atrial natriuretic peptide by a rabbit carotid artery smooth muscle cell. *Mol Endo* 1988;2:117–124.
42. Koehn JA, Norman JA, Jones BN, LeSueur L, Sakane Y, Ghai RD. Degradation of atrial natriuretic factor by kidney cortex membranes—isolation and characterization of the primary proteolytic product. *J Biol Chem* 1987;262:11623–11627.
43. Stephenson SL, Kenny AJ. The hydrolysis of α-human atrial natriuretic peptide by pig kidney microvillar membranes is initiated by endopeptidase-24.11. *Biochem J* 1987;243:183–187.
44. Cusson JR, DuSouich P, Hamet P, et al. Effects and pharmacokinetics of bolus injections of atrial natriuretic factor in normal volunteers. *J Cardiovasc Pharmacol* 1988;11:635–642.
45. Sonnenberg JL, Skane Y, Jengsinger AY, et al. Identification of protease

3.4.24.11 as the major atrial natriuretic factor degrading enzyme in the rat kidney. *Peptides* 1988;9:173–180.
46. Olins GM, Spear KL, Siegel NR, Reinhard EJ, Zurcher-Neely HA. Atrial peptide inactivation by rabbit-kidney brush-border membranes. *Eur J Biochem* 1987;170:431–434.
47. Gee NS, Bowes MA, Buck P, Kenny AJ. An immunoradiometric assay for endopeptidase-24.11 shows it to be a widely distributed enzyme in pig tissues. *Biochem J* 1985;228:119–126.
48. Krieter PA, Olins GM, Verrett SP, Durley RC. In vivo metabolism of atrial natriuretic peptide: identification of plasma metabolites and enzymes responsible for their generation. *J Pharmacol Exp Ther* 1989;249:411–417.
49. Seymour AA, Swerdel JN, Fennell SA, Druckman SP, Neubeck R, Delaney NG. Potentiation of the depressor responses to atrial natriuretic peptides in conscious SHR by an inhibitor of neutral endopeptidase. *J Cardiovasc Pharmacol* 1989;14:194–204.
50. Seymour AA, Fennell SA, Swerdel JN. Potentiation of renal effects of atrial natriuretic factor-(99-126) by SQ 29,072. *Hypertension* 1989;14:87–97.
51. Trapani AJ, Smits GJ, McGraw DE, et al. Thiorphan, an inhibitor of endopeptidase 24.11, potentiates the natriuretic activity of atrial natriuretic peptide. *J Cardiovasc Pharmacol* 1989;14:419–424.
52. Sybertz EJ, Chiu PJS, Vemulapalli S, et al. SCH 39370, a neutral metalloendopeptidase inhibitor, potentiates biological responses to atrial natriuretic factor and lowers blood pressure in desoxycorticosterone acetate-sodium hypertensive rats. *J Pharmacol Exp Ther* 1989;250:624–631.
53. Tremblay J, Huot C, Willenbrock RC, et al. Increased cyclic guanosine monophosphate production and overexpression of atrial natriuretic peptide A-receptor mRNA in spontaneously hypertensive rats. *J Clin Invest* 1993; 92:2499–2508.

(continued from page 5A)

FIRST IMPRESSIONS

REFLUX ESOPHAGITIS AS THE CAUSE OF ATYPICAL CHEST PAIN

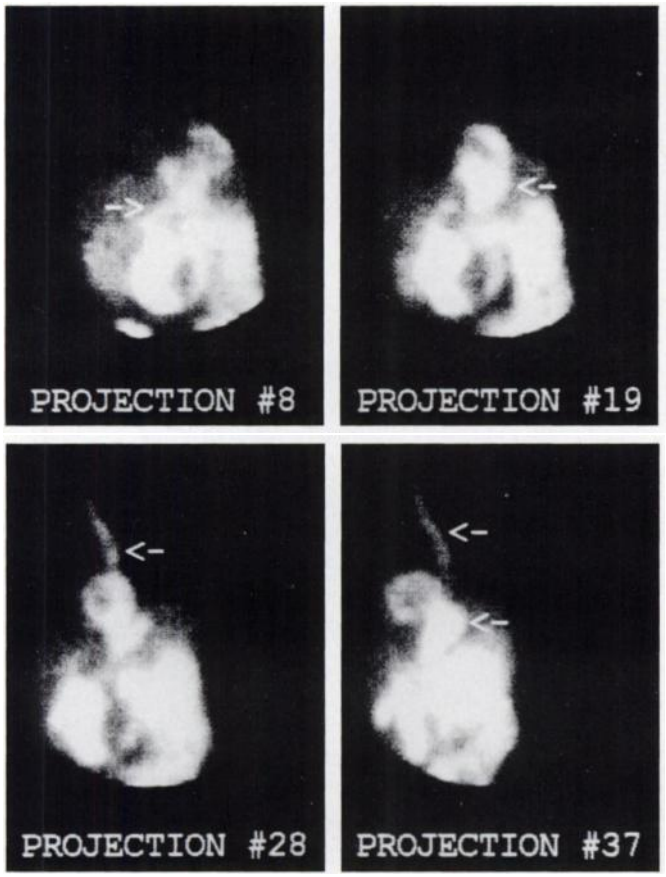

FIGURE 1.

PURPOSE
A 71-yr-old female with atypical chest pain was referred for a dipyridamole ^{99m}Tc-sestamibi stress test. During the test, she had no discomfort. There was no ECG evidence of ischemia. The processed SPECT images were unremarkable, without findings of ischemia or infarction. The unprocessed, individual SPECT projections, however, showed evidence of reflux of radiotracer from the gallbladder (projection 8) into the stomach (projection 19) and esophagus (projections 28 and 37). These images are compatible with reflux esophagitis as the cause of chest discomfort.

TRACER
Technetium-99m-sestamibi, 26.5 mCi (980 MBq)

ROUTE OF ADMINISTRATION
Intravenous

IMAGING TIME AFTER INJECTION
Ninety minutes. The patient drank 8 oz of whole milk approximately 30 minutes prior to imaging.

INSTRUMENTATION
ADAC ARC 4000 gamma camera and Pegasys computer system (64 x 64 x 16 matrix; 64 views at 20 sec/view).

CONTRIBUTORS
Mark I. Travin, Diane D. Demus, Nancy Grant, William S. Klutz

INSTITUTION
Roger Williams Medical Center, Brown University School of Medicine, Providence, RI